

Instantaneous Radio Spectra of Giant Pulses from the Crab Pulsar from Decimeter to Decameter Wavelengths

M.V. Popov¹, A.D. Kuz'min², O.M. Ul'yanov³, A.A. Deshpande^{4,5}, A.A. Ershov², V.V. Zakharenko³, V.I. Kondrat'ev¹, S.V. Kostyuk¹, B.Ya. Losovskij², and V.A. Soglasnov¹

1-Astro Space Center, Lebedev Physical Institute, Russian Academy of Sciences, Profsoyuznaya ul. 84/32, Moscow, 117997 Russia; 2-Pushchino Radio Astronomy Observatory, Astro Space Center, Lebedev Physical Institute, Russian Academy of Sciences, Pushchino, Moscow oblast, 142290 Russia; 3-Institute of Radio Astronomy, National Academy of Sciences of Ukraine, Krasnoznamennaya ul. 4, Kharkov, 61002 Ukraine; 4-Raman Research Institute, C.V. Raman Av., Sadashivanagar, Bangalore, 560 080 India; 5-Arecibo Observatory, HC03 Box 53995, Arecibo, 00612 Puerto Rico

Abstract

The results of simultaneous multifrequency observations of giant radio pulses from the Crab pulsar, PSR B0531+21, at 23, 111, and 600 MHz are presented and analyzed. Giant pulses were detected at a frequency as low as 23 MHz for the first time. Of the 45 giant pulses detected at 23 MHz, 12 were identified with counterparts observed simultaneously at 600 MHz. Of the 128 giant pulses detected at 111 MHz, 21 were identified with counterparts observed simultaneously at 600 MHz. The spectral indices for the power-law frequency dependence of the giant-pulse energies are from -3.1 to -1.6 . The mean spectral index is -2.7 ± 0.1 and is the same for both frequency combinations (600–111 MHz and 600–23 MHz). The large scatter in the spectral indices of the individual pulses and the large number of unidentified giant pulses suggest that the spectra of the individual giant pulses do not actually follow a simple power law. The observed shapes of the giant pulses at all three frequencies are determined by scattering on interstellar plasma inhomogeneities. The scatter-broadening of the pulses and its frequency dependence were determined as $\tau_{sc} = 20(\nu/100)^{-3.5 \pm 0.1}$ ms, where the frequency ν is in MHz.

1. INTRODUCTION

The Crab Nebula pulsar, PSR B0531+21, was discovered by Staelin and Reifenstein [1] in 1968 via the detection of its anomalously strong pulses. Such pulses were subsequently called giant pulses. Their peak fluxes are factors of hundreds to thousands the peak fluxes in an average pulse formed by the synchronous integration of the pulsar signal with the neutron star rotation period, which is approximately 33 ms for PSR B0531+21. Giant pulses (GPs) of radio emission have been detected in several pulsars: first in the millisecond pulsar B1937+21 [2, 3], then in the millisecond pulsars J1824–2452 [4], B0540–69 [5], B1957+20, and J0218+4232 [6], as well as the millisecond pulsar J1823–3021A in the globular cluster NGC 6624 [7]. GPs were also detected in the ordinary pulsars B0031–07 [8], B1112+50 [9], and J1752+2359 [10]. In all these pulsars, GPs are observed fairly rarely, and their properties remain poorly studied. The GPs from the Crab pulsar (see, e.g., the brief review of Hankins [11]) and the millisecond pulsar B1937+21 [12–14] have been studied in more detail. Together with their high peak flux density, which exceed a hundred thousand Jy at decimeter wavelengths, the GPs from PSR B0531+21 have an extremely short duration. Hankins et al. [15] found the outbursts in this pulsar to be shorter than 2 ns at 5.5 GHz. Such nanopulses have brightness temperatures exceeding 10^{37} K. Still higher brightness temperatures (5×10^{39} K) have been obtained for GPs from the millisecond pulsar B1937+21 [14]. Thus, the properties of GPs suggest a highly efficient radio emission mechanism, and analyzing these properties can improve our understanding of the nature of this coherent mechanism.

One important characteristic of GPs is their radio spectrum. GPs were detected from B0531+21 at all frequencies at which they were searched for. GPs were first detected at 112 MHz [1], while Hankins [11] mentions an observation of one GP at 15 GHz. Simultaneous observations of GPs at several frequencies are of primary interest, since they make it possible to obtain instantaneous spectra of individual pulses. Sallmen et al. [16] published the results of simultaneous observations of GPs from PSR B0531+21 at 1400 MHz (VLA) and 600 MHz (the 25-m Green Bank telescope) in 1999. Approximately 70% of the GPs detected at 1400 MHz were also detected at 600 MHz. The spectral indices of such pulses were from -4.9 to -2.2 . This same paper reports the results of simultaneous observations at 1.4 and 4.9 GHz, which yielded spectral indices from -4 to 0 . Thus, although the average GP spectral index was close

to that for the components of the average pulse profile (according to Moffett [17], this value is -3.0 in the frequency band considered), the instantaneous spectra of individual GPs varied over fairly broad ranges, indicating that the GP radio spectrum has a complex character that cannot be described by a simple power law. We report here the results of our analysis of instantaneous spectra of radio GPs from PSR B0531+21 measured using simultaneous observations at 23.23 MHz (the UTR-2 radio telescope in Kharkov), 111.87 MHz (the LPA radio telescope in Pushchino), and 600.0 MHz (the 64-m radio telescope in Kalyazin).

2. OBSERVATIONS AND DATA REDUCTION

The observations were carried out on November 24–26, 2003, as part of an international program of multifrequency studies of GPs from the Crab pulsar. In addition to the radio telescopes mentioned in the Introduction, GP observations were also conducted on the 100-m radio telescope at Effelsberg (8350 MHz), the 76-m radio telescope of Jodrell Bank Observatory (1400 MHz), and the Westerbork Synthesis Radio Telescope (1200 MHz). A complete analysis of the multifrequency observations will be presented in other publications.

2.1. 23 MHz

The 23 MHz observations were conducted on the UTR-2 radio telescope. This telescope is T-shaped, and consists of three segmented antennas: southern (S), northern (N), and western (W), corresponding to their directions from the UTR-2 phase center. The UTR-2 construction includes broadband Nadeenko dipoles, which are sensitive to radiation with east–west linear polarization. The total number of the UTR-2 oscillators is 2040. For more details about the UTR-2 telescope and its system of amplifiers, see [18, 19]. We used a dual-channel reception system. The signal summed from the S and N (S+ N) antennas was fed to the first channel of the receiver, while the second channel was connected to the output of the western antenna (W). This usage of the antennas enabled us to have an additional criterion for GP detection, based on comparing the output signals from the two channels. We chose identical receiving frequencies for the two channels, which enabled us to form sum and difference beams for the S+N and W antennas.

We used the dual-channel Portable Pulsar Receiver (PPR) designed at the Raman Research Institute (Bangalore, India). This receiver has an internal rubidium standard and a frequency synthesizer, which ensures both channels operate synchronously. The receiver implements digital heterodyning of the intermediate-frequency signals and four-level (two-bit) quantization of the output signal with a time step of 325 ns. A detailed description of this receiver can be found on the web site of the Raman Research Institute [20]. The system noise temperature was determined by the Galactic background radiation in the main lobe of the antenna beam, the radio emission of the Crab Nebula itself, and the noise of the receiving system itself. According to Roger et al. [21], the brightness temperature of the Galactic background toward the Crab Nebula in the 23–24 MHz band is 40 000 K. The noise of the UTR-2 radio telescope adds 4000–5000 K. The contribution of the Crab Nebula to the noise temperature in this frequency band is about 3000 Jy. The non thermal point like radio source (pulsar) contributes another 1000 Jy [22]. It is difficult to make an accurate calibration and estimation of the UTR-2's sensitivity toward the Crab pulsar. At 23–24 MHz and with the specified UTR-2 configuration, the Crab Nebula is unresolved. Therefore, observations at decameter wavelengths reveal rapid scintillations on inhomogeneities in the interplanetary plasma and ionosphere. We must also take into account the change in the radio telescope's effective area due to its tracking of the pulsar. When estimating the actual sensitivity of the UTR-2, we compared the radio telescope's response in the calibration mode toward the pulsar with the response from a reference noise generator placed at the phase center of the radio telescope. A similar comparison was done in additional observations of the Galactic background near the Crab Nebula. The main beam of the radio telescope was shifted from the Crab Nebula by approximately 2° in four directions. To remove the effect of scintillations on the sensitivity estimate and to correctly determine the background level, we smoothed the data obtained over intervals of two hours. This approach allowed us to estimate more correctly the brightness temperature of the Galactic background in directions near that toward the pulsar; according to our estimates, this is $50\,000 \pm 4000$ K at 23–24 MHz. Given the additional noise from the Crab Nebula and point source, we estimated the noise toward the pulsar recalculated to flux density units to be approximately 9000 Jy. Taking into account the averaging of the signal over the

receiver bandwidth (1.5 MHz) and in time (0.26624 s), we estimated the sensitivity, i.e., the rms deviation of the signal in flux-density units, to be 15 Jy in the individual-GP detection mode. Given the calibration errors and influence of scintillations, we believe the uncertainty of this estimate does not exceed 30%. The effect of dispersion of the radio waves was removed using the method of coherent dedispersion [23]. We used the dispersion measure of 56.757 pc/cm^3 from the Jodrell Bank Crab Pulsar Monthly Ephemeris [24] when reconstructing the signal. At $f_0 = 23 \text{ MHz}$ and with $\Delta f = 1.538 \text{ MHz}$, the dispersive pulse broadening in the interstellar plasma for the pulsar's dispersion measure of 56.757 pc/cm^3 is $\Delta t = 52.5 \text{ s}$. When restoring the signal via coherent dedispersion on the time interval T , a data segment of duration Δt will be lost at the beginning or end of the time interval T , depending on whether the dedispersion is applied to the lower or upper end of the frequency band with width Δf . Therefore, the time interval T on which the dedispersion is implemented must appreciably (by at least a factor of two) exceed Δt . We performed dedispersion in ten passes, each time compensating for one-tenth of the total dispersion measure. In this approach, the time interval T was 10.9052 s, and the time Δt for $\text{DM} = 5.6757 \text{ pc/cm}^3$ was 5.253 s. The data file for the Fourier transform contained 33 554 432 elements. Since the expected temporal scattering on inhomogeneities in the interstellar plasma was several seconds, we analyzed the reconstructed signal with averaging over a time interval of 0.26624 s. Before the detection of the first obvious GP, the reconstructed signal was examined by eye; we subsequently applied an automated procedure to identify events based on the calculated convolution of the restored signal with a template corresponding to the shape of the detected pulse. A formal 5σ detection criterion was established for values of the calculated convolution. Our subsequent analysis showed that using a 5σ detection criterion yields fewer than 10% false GPs. This analysis was conducted by comparing the number of events detected in the signal restored with the final dispersion measure (56.757 pc/cm^3) and the number of events detected in the signal at an intermediate stage, with a dispersion measure of 45.4 pc/cm^3 .

The time alignment of the 23 MHz observations was brought about by inserting time stamps tied to the time service of the observatory into the first channel of the receiver. The clock rate of the time service was checked using GPS signals before each observing session.

The time-stamp repetition period was 10 s, the time-stamp duration was 20 ms, and a longer stamp with duration of 100 ms was inserted at each whole minute. The formal accuracy of the time alignment of the recorded data was about 0.1 ms. The effective width of a GP was 4.0 s. The actual accuracy of the time alignment of the detected GPs is determined by the duration of the leading edges of these pulses, which is about 1 s.

2.2. 111 MHz

The observations were carried out on the Large Phased Array (LPA) transit radio telescope of Pushchino Radio Astronomy Observatory (Astro Space Center, Lebedev Physical Institute), which has an effective area at the zenith of about 15000 m². The flux sensitivity of the system measured on discrete sources and pulsars with known fluxes was $\sigma_s \approx 200 \text{ mJy MHz}^{-1} \text{ s}^{-1}$ (toward an area of sky with a brightness temperature of 1000 K). One linear polarization was received. A 64-channel receiver with channel bandwidth $\Delta f = 20 \text{ kHz}$ was utilized. The total frequency bandwidth was 1.28 MHz. The frequency of the first (highest frequency) channel was 111.87 MHz. The sampling interval was 8.2 ms. The time constant $\tau = 10 \text{ ms}$. Individual pulses were recorded. The observations were processed in an automated mode. The records were cleaned of interference, and inter channel compensation for the dispersion delay was applied. Pulses exceeding the noise level by 5σ were identified, and their amplitudes, phases, and pulse widths determined. We confirmed a pulse belonging to the pulsar by processing the observational data after splitting it into groups with different frequency channels, to check whether the pulse was present in each group and with the expected dispersion delay. Another test was processing with a varying dispersion measure. If a pulse is associated with the pulsar, the pulse amplitude and signal-to-noise ratio will be maximum when processed with the nominal dispersion measure, $DM = 56.757 \text{ pc/cm}^3$. The flux density was calibrated using observations of the pulsar PSR B1919+21, for which all the parameters of the LPA beam pointing are identical to those for the Crab Pulsar. We used 12 observing sessions for PSR B1919+21, whose 111-MHz flux density we took to be 1.55 Jy.

The time alignment of the observations at 111 MHz was done using a rubidium standard of the observatory time service controlled by TV signals from the State Time and Frequency Standard. The timing accuracy was better than 100 μs . The measured effective pulse width due

to scattering was 25 ms. The accuracy of the pulse arrival time at this frequency is limited to 2 ms by scattering.

2.3. 600 MHz

The observations at 600 MHz were conducted on the TNA-1500 radio telescope in Kalyazin. The radio emission was received in two channels with left-hand and right-hand circular polarizations (LCP and RCP). Two 4-MHz frequency bands (upper and lower side bands) were recorded in each polarization channel. The central frequency was 600.0 MHz. The time resolution was 250 ns. The data were recorded on video cassettes in a two-bit binary code using the S2 recording system. The data were played back after the observations at the Astro Space Center of the Lebedev Physical Institute on a specialized S2-RDR system designed in the Astrophysical Data Processing Department of the Astro Space Center. The equivalent system temperature was 1300 Jy due to the contribution of the radio emission from the Crab Nebula [25]. To improve the sensitivity of the GP search, we averaged the signal over 256 points ($32 \mu\text{s}$), since the temporal broadening of the pulses due to scattering on inhomogeneities of the interstellar plasma is about $50 \mu\text{s}$ at 600 MHz. With this averaging, the 1σ fluctuation sensitivity was 110 Jy. In the GP searches, we combined the signals in the four recorded channels, so that the resulting minimum detectable peak GP flux was 420 Jy. The techniques used for the data processing and the GP detection criteria are described in our previous publication [26]. The time alignment of the 600-MHz observations was achieved with a hydrogen standard of the observatory time service controlled by TV signals of the State Time and Frequency Standard and by GPS signals. The timing accuracy was $0.1 \mu\text{s}$. At this frequency, the accuracy of the pulse arrival times is limited to $10 \mu\text{s}$ by scattering. The average GP profile at 600 MHz with a time resolution of $4 \mu\text{s}$ is presented in the figure.

Observational data

Frequency, MHz	600.0	111	23.23
Observation time, h	36	0.25	12
Number of detected GPs	40200	128	45
Number of identified GPs	-	21	12

τ_{sc} , ms	0.043 ± 0.005	15 ± 3	3000 ± 1000
$S^{\text{peak}}(\text{min})$, Jy	420	60	75
$S^{\text{peak}}(\text{max})$, Jy	34000	700	150
E_{max} , Jy ms	2000	17000	600000

3. RESULTS

The table lists the main observational parameters: the total observing time at each frequency, number of detected GPs, number of GPs at 111 and 23 MHz identified with counterparts at 600 MHz, pulse scatter-broadening τ_{sc} , minimum peak flux density of detectable GPs $S^{\text{peak}}(\text{min})$, maximum peak flux density of the observed GPs $S^{\text{peak}}(\text{max})$, and radiation energy of the strongest GP E_{max} . We carried out three observing sessions. The total duration of the 23 MHz sessions was about 1 300 000 pulsar periods. During this time, 45 GPs with peak flux densities exceeding 7.5 Jy, or with energies above 300 000 Jy ms, were recorded (1 GP per approximately 30 000 pulsar periods). No GPs were detected at 23 MHz during the time common with the 111-MHz observations. In the three observing sessions at 111 MHz (about 4 min each), which included about 20 000 pulsar periods, 128 GPs with peak flux densities exceeding 60 Jy, or with energies above 2000 Jy ms, were recorded (approximately 1 GP per 160 pulsar periods). The energy of the strongest GP exceeds the energy of the average pulsar pulse by a factor of approximately 40–50. The total duration of the Kalyazin observations was 36 h; 40 200 GPs with peak flux densities exceeding 420 Jy, or with energies above 25 Jy ms, were recorded (1 GP per approximately 100 pulsar periods); 518 were observed during the time that was common with the 111-MHz observations. The smaller number of GPs detected at the lower frequencies is due to the decrease in the peak flux density of the observed GPs due to pulse scatter broadening and the increase in the brightness temperature of the Galactic background. Therefore, only the most intense GPs were detectable at those frequencies. The figure shows examples of individual GPs at each frequency (left), together with the average GP profiles (right). The time resolutions in this figure are 0.26624 s, 8 ms, and 4 μ s for 23, 111, and 600 MHz, respectively. The average GP profile at 23 MHz was obtained by averaging the ten strongest pulses, which were time-aligned using the maximum of the convolution used in the

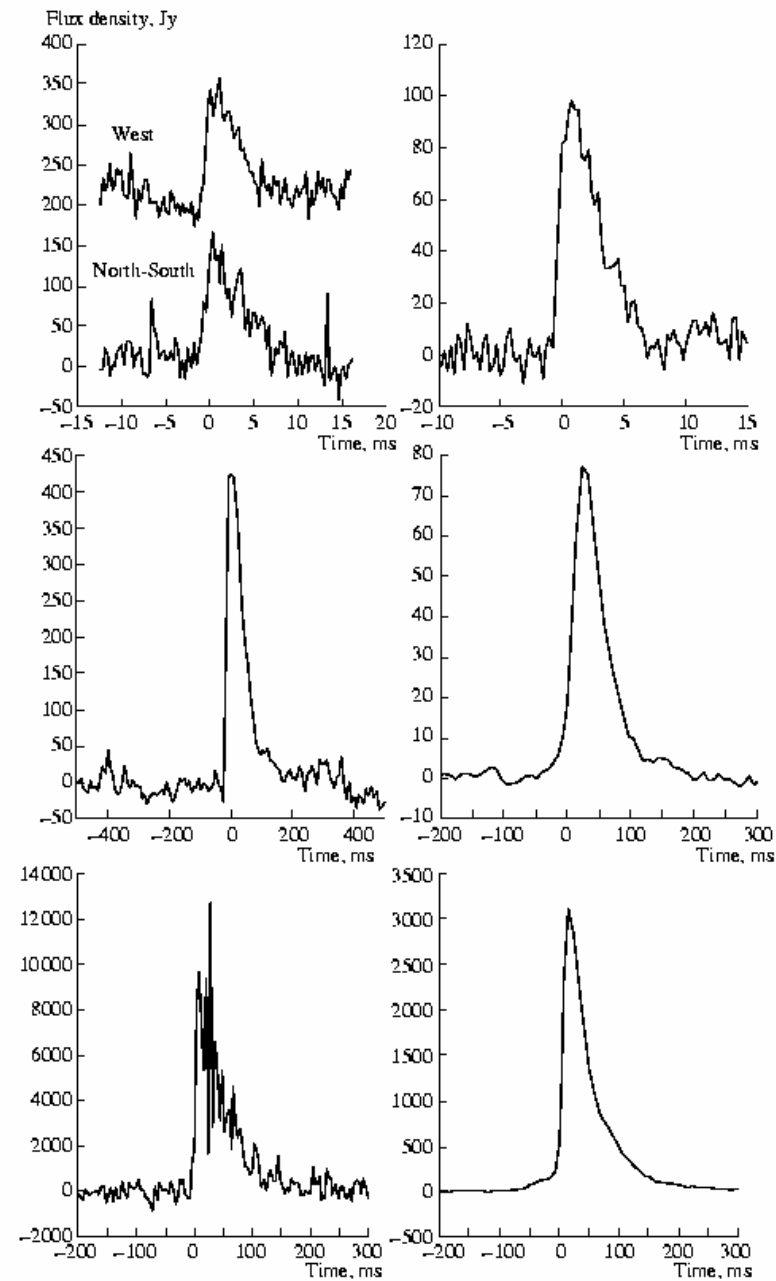
GP search at this frequency. The average GP profile at 600 MHz was obtained by averaging all strong pulses with peak flux densities exceeding 1000 Jy. With such averaging, the individual pulses were aligned using a point at the leading edge, for which the maximum deviation from the mean was less than 30% of the maximum amplitude of this pulse on a record averaged over 4 μ s. The shapes of the average pulses at all three frequencies are produced by scattering on inhomogeneities of the interstellar plasma. GPs were identified at different frequencies based on coincidence of the pulse arrival times translated to an infinitely high frequency using the dispersive delay and the dispersion measure of 56.757 pc/cm³. We identified 21 simultaneous GPs at 600 and 111 MHz. The spectral indices in the frequency dependence for the energies of these GPs are from -3.1 to -1.6; the mean spectral index is -2.7 ± 0.1 . The spectral index for these frequencies for pulses observed at the detection limit is -2.6. Since most of the GPs detected at 600 and 111 MHz remained unidentified, we conclude that 95% of pulses detected at 600 MHz have spectral indices relative to 111 MHz that are less steep than -2.6, while 85% of GPs detected at 111 MHz have spectral indices steeper than -2.6. The most interesting result of our observations is the detection of GPs at 23 MHz. When identifying them with counterparts detected at 600 MHz, we took GPs at detected at 23 and 600 MHz within a 1-s interval to be simultaneous. To reduce the number of spurious identifications with GPs at 600 MHz, which are detected approximately every 3 s, we identified events at 23 MHz only with strong pulses at 600 MHz exceeding the 10 σ level (1100 Jy). Only two identifications were expected if the events were random. We identified 12 simultaneous events. The spectral indices in the frequency dependence of the energies of these identified GPs range from -3.1 to -2.5. The mean spectral index is -2.7 ± 0.1 . This value of the spectral index should be treated with caution, since it is subject to selection effects. We compared at both frequencies a small number of pulses that exceeded the adopted detection limit. For pulses whose energies matched the detection limits at both frequencies, the spectral index is -2.6, while pulses with spectral indices that differ appreciably from this value will not be observable at one or the other frequency. Since we detected about 1500 GPs with peak flux densities above 10 σ during 12 h of simultaneous observations at 600 MHz, and only 12 of these pulses were identified with events at 23 MHz, the overwhelming

majority of GPs detected at 600 MHz have spectral indices less steep than -2.6 . On the other hand, an appreciable fraction of GPs detected at 23 MHz (about two-thirds) have spectral indices steeper than -2.6 . Our detection of giant pulses at 23 MHz has expanded measurements of the frequency dependence of the pulse scatter-broadening to decameter wavelengths. GPs are observed as very infrequent isolated pulses with large intensities, far exceeding the mean level of the pulsar radio emission. This distinguishes GPs from the regular sequence of ordinary pulses, eliminates the effect of subsequent pulses, and enables measurements at low frequencies, where the pulse scatter-broadening exceeds the pulsar period. The pulse scatter-broadening was determined by comparing the observed average GP profile with a model scattered template representing the initial pulsar pulse. A Gaussian pulse was taken for this template. The template pulse was “scattered” by convolving it with a truncated exponential function, corresponding to scattering in a thin screen. The observed pulsar pulse was least-squares fit using this model scattered pulse to derive the scatter broadening τ_{sc} , amplitude, width, and time delay of the template pulse. The average GP profile at 111 MHz was obtained from observations with higher time resolution done on days adjacent to the simultaneous observations. The table lists our measurements of the pulse scatter-broadening. A least-squares fit yields the frequency dependence $\tau_{\text{sc}} = 20(\nu/100)^{-3.5 \pm 0.1}$ (where τ_{sc} is in ms and ν in MHz), which matches well broader-band measurements of the frequency dependence of scattering for this pulsar [27]: $\tau_{\text{sc}} = 22(\nu/100)^{-3.8 \pm 0.2}$.

4. CONCLUSIONS

We have performed simultaneous observations of giant pulses in the Crab pulsar (PSR B0531+21) radio emission at 600, 111, and 23 MHz, and detected giant pulses at 23 MHz for the first time. Thus, the mechanism generating the giant pulses extends to decameter wavelengths. The mean spectral index of the frequency dependence for the energy of the identified pulses is $\alpha = -2.7$, and is the same when calculated for the 600–111 and 600–23 MHz data. The considerable range of variations in the GP spectral indices and large number of unidentified pulses suggest that representing the instantaneous spectra of the giant radio pulses of PSR B0531+21 using a simple power law does not describe the true shape of the

radio spectrum of these pulses, which may have a complex form. We have measured the pulse scatter-broadening and its frequency dependence: $\tau_{\text{sc}} = 20(\nu/100)^{-3.5 \pm 0.1}$. The exponent of this power law differs from the values predicted either by a Kolmogorov model for the spectrum of the inhomogeneities in the scattering plasma (-4.4) or a Gaussian model (-4.0). We attribute this fact to a considerable contribution of the Crab Nebula itself to scattering of the pulsar radio emission.



A strong GP recorded at 23 MHz in the two channels of the UTR-2 radio telescope (upper left). The short periodic spikes in the lower curve reflect the 10-s time signals injected into the receiving channel for the time alignment. Average profile of GPs at 23 MHz obtained by averaging ten strongest pulses in the channel connected to the western arm of the UTR-2 antenna (upper right). The middle and lower panels show examples of an individual GP (left) and average GP profile (right) at 111 and 600 MHz, respectively.

REFERENCES

1. D.H. Staelin and E.C. Reifenstein III, *Science* 162, 1481 (1968).
2. A. Wolszczan, J.M. Cordes, and D.R. Stinebring, *Millisecond Pulsars*, Ed. by S. P. Reinolds and D. R. Stinebring (NR AO, Green Bank, 1984), p. 63.
3. S. Sallmen and D.C. Backer, in *Millisecond Pulsars. A Decade of Surprise*, Ed. by A.S. Fruchter, M. Tavani, and D.C. Backer, *Astron. Soc. Pac. Conf. Ser.* 72, 340 (1995).
4. R.W. Romani and S. Johnston, *Astrophys. J.* 557, L93 (2001).
5. S. Johnston and R.W. Romani, *Mon. Not. R. Astron. Soc.* 332, 109 (2002).
6. B.C. Joshi, M. Kramer, A.G. Lyne, et al., in *IAU Symp. No. 218: Young Neutron Stars and Their Environments*, Ed. by F. Camilo and B. M. Gaensler (Astron. Soc. Pac., San Francisco, 2004), p. 68.
7. H.S. Knight, M. Bailes, R.N. Manchester, et al., *Astrophys. J.* 625, 951 (2005).
8. A.D. Kuz'min, A.A. Ershov, and B.Ya. Losovskii, *Pis'ma Astron. Zh.* 30, 285 (2004) [*Astron. Lett.* 30, 247 (2004)].
9. A.A. Ershov and A.D. Kuz'min, *Pis'ma Astron. Zh.* 29, 111 (2003) [*Astron. Lett.* 29, 91 (2003)].
10. A.A. Ershov and A.D. Kuzmin, *Astron. Astrophys.* 443, 593 (2005).
11. T.H. Hankins, in *Pulsar Astronomy—2000 and Beyond*, Ed. by M. Kramer, N.Wex, and R. Wielebinski, *Astron. Soc. Pac. Conf. Ser.* 202, 165 (2000).
12. I. Cognard, J.A. Shrauner, J.H. Taylor, and S.E. Thorsett, *Astrophys. J.* 457, L81 (1996).
13. A. Kinkhabwala and S.E. Thorsett, *Astrophys. J.* 535, 365 (2000).
14. V.A. Soglasnov, M.V. Popov, N. Bartel, et al., *Astrophys. J.* 616, 439 (2004).
15. T.H. Hankins, J.S. Kern, J.C. Weatherall, and J.A. Eilek, *Nature* 422, 141 (2003).
16. S. Sallmen, D.C. Backer, T.H. Hankins, et al., *Astrophys. J.* 517, 460 (1999).
17. D.A. Moffett, PhD Thesis (New Mexico Institute Mining and Technology, 1997).
18. A.V. Men', L.G. Sodin, N.K. Sharykin, et al., *Antenny*, No. 26, 15 (1978).
19. E.P. Abranin, Yu.M. Bruk, V.V. Zakharenko, and A.A. Konovalenko, *Exp. Astron.* 11, 85 (2001).
20. <http://www.rri.res.in/dspiral/ppr/hardware/hardware.htm>.

21. R.S. Roger, C.H. Costain, T.L. Landecker, and C. M. Swerdlyk, *Astron. Astrophys.*, Suppl. Ser. 137, 7 (1999).
22. A.L. Bobeiko, V.P. Bovkoon, S.Ya. Braude, et al., *Astrophys. Space Sci.* 66, 211 (1979).
23. T.H. Hankins, *Astrophys. J.* 169, 487 (1971).
24. <http://www.jb.man.ac.uk/pulsar/crab.html>.
25. S.V. Kostyuk, V.I. Kondrat'ev, A.D. Kuz'min, et al., *Pis'ma Astron. Zh.* 29, 440 (2003) [*Astron. Lett.* 29, 387 (2003)].
26. M.V. Popov, V.A. Soglasnov, V.I. Kondrat'ev, et al., *Astron. Zh.* 83, 62 (2006) [*Astron. Rep.* 50, 55 (2006)].
27. A.D. Kuz'min, V.I. Kondrat'ev, S.V. Kostyuk, et al., *Pis'ma Astron. Zh.* 28, 292 (2002) [*Astron. Lett.* 28, 251 (2002)].